Evaluation of SPET quantification of simultaneous emission and transmission imaging of the brain using a multidetector SPET system with the TEW scatter compensation method and fan-beam collimation

Takashi Ichihara[1], Nobutoku Motomura[1], Koichi Ogawa[2], Hyoji Hasegawa[1], Jun Hashimoto[3], Atushi Kubo[3]

[1] Toshiba Medical Engineering Laboratory, 1385 Shimoishigami, Otawara-shi, Tochigi-ken, Japan
[2] Department of Electrical Engineering, College of Engineering, Hosei University, Koganei-shi, Tokyo, Japan
[3] Keio University School of Medicine, Tokyo, Japan

Received 2 February and in revised form 22 April 1996

Abstract. A gamma camera system which is able to acquire simultaneous single-photon emission tomographic (SPET) data and gamma ray transmission computed tomography (TCT) data for brain study using external rod sources and fan-beam collimators was developed and evaluated. Since the three external rod sources were located at the focal points of fan-beam collimators, which also happened to be the apexes of the equilateral triangle defined by the three detectors, simultaneous SPET and TCT scan could be performed using a 120° shared scan. Therefore, the proposed system required less than one-third of the scanning time of a single-head system. Since the combination of rod sources and fan-beam collimators decreased the scatter component in transmission data without a slit collimator for each rod source, the radioactivity of the rod source was less than one-tenth of the previous investigations. For evaluation, we used two isotopes, thallium-201 for TCT and technetium-99m for SPET. The cross-contamination of transmission and emission was well compensated using the triple energy window (TEW) method. In a separate TCT scan, the measured attenuation coefficient of ^{201}Tl for water was 0.19±0.01 cm^{-1}, while in a simultaneous scan, it was 0.20±0.01 cm^{-1}. The measured attenuation coefficient for water agreed well with the narrow-beam (theoretical) value of 0.187 cm^{-1}. In SPET images, scatter compensation was also performed using the TEW method and attenuation compensation was done using the measured attenuation map. The results showed the feasibility of simultaneous SPET and TCT scanning using the TEW method to obtain quantitative SPET images.

Key words: Single-photon emission tomographic quantification – Transmission measurement – Scatter compensation – Attenuation compensation – Fan-beam collimator – TEW method

Correspondence to: T. Ichihara, Toshiba Medical Engineering Laboratory, 1385 Shimoishigami, Otawara-shi, Tochigi-ken, Japan

Eur J Nucl Med (1996) 23:1292–1299

Introduction

Photon attenuation is one of the most important factors degrading the quantitative accuracy of single-photon emission tomography (SPET) images. Precise information about attenuation distribution is needed for accurate attenuation compensation. Recently, numerous methods for the measurement of attenuation distribution using transmission computed tomography (TCT) scans have been reported [1–6]. The simultaneous SPET and TCT scan with dual isotopes, which is possible in SPET but not in positron emission tomography, was investigated as a way to avoid the problems of misalignment between SPET images and TCT images and longer scan time for clinical applications. However, there is scatter from emission data to transmission data and from transmission data to emission data. In previous research, scatter compensation of transmission data and attenuation compensation using broad-beam measurement have been performed in simultaneous emission and transmission imaging. The scatter compensation of emission data was performed using a point spread function (PSF) of scattered photons in simultaneous emission and transmission imaging and sufficient accuracy was achieved. PSF depends on the primary photon energy, order of Compton scattering, energy window width and collimator characteristics (septal thickness, penetration and hole diameter) [16]. PSF must be measured using a phantom with similar geometry and position in clinical use [15]. A scanning line source method has been developed for measurement of attenuation coefficient using a narrow beam instead of using a broad beam [8]. Methods have been developed for simultaneous acquisition of emission and transmission on triple-head SPET system, using long-fo-

cus (114 cm [7], 50–65 cm [17]) fan-beam collimators. A scanning procedure requires each detector to scan 240° or 360°.

In this study, we designed and evaluated a simultaneous emission and transmissinon scan system for brain SPET using the triple energy window (TEW) scatter compensation method [9, 10, 14] and fan-beam collimators. We designed the detector and fan-beam collimator geometry in which the rod sources for TCT were located at the apexes of the equilateral triangle defined by the three detectors, and these apexes were at the focal position of fan-beam collimators.

Regional energy spectra of the transmission data were measured pixel by pixel to confirm the reduction in scattered photons with a fan-beam collimator and line source. Evaluation of TCT images obtained using the proposed method was performed in comparison with both the theoretical values and the measured values in separate TCT scans. In addition, to evaluate the quality of simultaneous SPET images compensated using the proposed method, these images were compared with SPET images compensated using two other methods. One method was "broad-beam uniform attenuation compensation" using an empirical attenuation value without scatter compensation [13], and the other was "narrow-beam uniform attenuation compensation" using a narrow-beam (theoretical) attenuation value with scatter compensation.

Materials and methods

System overview. If the objective of a SPET system is focused on brain studies, optimization of spatial resolution of SPET images and attenuation measurement by TCT is possible. The following triple-headed SPET camera was designed. As shown in Fig. 1, an external rod source #1 (radioisotope container) for TCT is located at one of the apexes of the equilateral triangle which is defined by detectors #2 and #3. This apex is at the focal position of the fan-beam collimator #1. Likewise the external sources #2 and #3 are at the focal positions of the fan-beam collimators #2 and #3, respectively. The proposed geometry formed by the fan-beam collimators has the following merits:

1. Simultaneous SPET and TCT scans can be performed with the 120° shared scan using conventional fan-beam collimators. The proposed system requires less than one-third of the scanning time of a single-head system.
2. The combination of the rod sources and the fan-beam collimators decreases the scatter component in transmission data without a slit collimator and thus provides a narrow-beam attenuation measurement of subjects. This was proven by pixel by pixel measurement of the regional energy spectra of the transmission data.

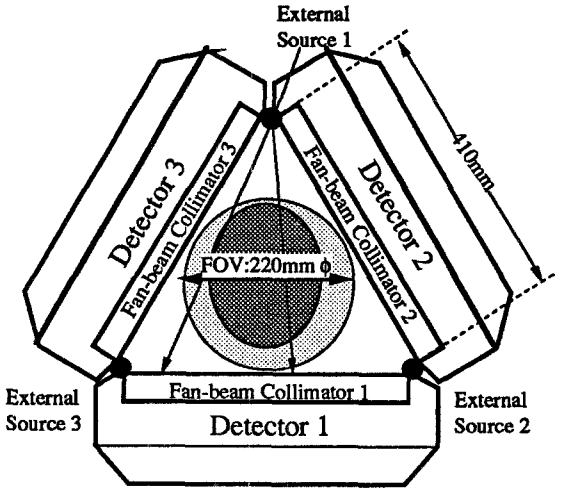

Fig. 1. Geometric configuration of the simultaneous SPET/TCT system

The system shown in Fig. 1 has the following major components:

1. Three rod sources containing an appropriate gamma emitter
2. Three fan-beam collimators
3. Three scintillation cameras with a rectangular field of view (410 mm×210 mm)
4. Multi-energy window acquisition

The main components are mounted on a Toshiba GCA-9300A/HG triple-head SPET camera. The external source assembly is a 35-cm-long plastic tube (8-mm inside diameter and 12-mm outside diameter). The rod is filled with a radioisotope; one end is closed and the other end is sealed using a metal cap equipped with a small O-ring. In this work, the radioactivity of the external source was 85 MBq/rod (2.43 MBq/cm) of thallium-201. The slit collimator was not attached to the external rod source for transmission data acquisition. The SPET field of view is a cylinder with diameter 220 mm and axial length 210 mm. SPET data and TCT data are acquired over 360° by performing shared scanning, in which each detector rotates through 120°. The super-high-resolutin (SHR) fan-beam collimator used in this work has a focal length of 397 mm, a septal thickness of 0.1 mm and a central hole length of 40 mm. Volume sensitivity was 34.8 kcps/(MBq/ml)/cm and tomographic spatial resolution was 7.8 mm FWHM at the centre [11]. For comparison, in the case of the single-head SPET system with a high-resolution parallel hole collimator under the same measuring conditions, volume sensitivity and tomographic spatial resolution were 11.3 kcps/(MBq/ml)/cm and 10.2 mm (FWHM), respectively.

Brain phantom. The brain phantom (long axis 196 mm, short axis 158 mm, thickness 60 mm) used in this work consisted of tissue and skull (thickness 8 mm) parts. The tissue part was filled with water (white matter 300 ml, grey matter 530 ml: ECT Brain Phantom IB-30, Kyoto Kagaku Hyouhon Corporation, Kyoto, Japan). The elemental composition of skull substitute material was: H 3.69%, C 29.22%, N 1.19%, O 32.66%, P 10.24%, C 10.06%, Ca 22.92%. The elemental composition of standard bone is: H 3.39%, C 15.50%, N 3.97%, O 44.10%, Na 0.06%, Mg 0.21%, P 10.20%, S 0.31%, Ca 22.20% [19]. We simulated acquisition conditions of a technetium-99m hexamethylpropylene amine oxime (HMPAO) brain study (740 MBq, 30-min scan). The cortex and thalamus compartments of the phantom were filled with ^{99m}Tc (300 kBq/ml) and the white matter compartment with 109 kBq/ml.

Regional energy spectrum acquisition. Figure 2 shows the block diagram of the regional energy spectrum acquisition mode. The position of a photon detected by the gamma camera is shown as (x, y). The energy channel of the photon is shown as n. The detected photons are compensated for energy and linearity; those within the previously set energy range (E_{lower} to E_{upper}) are separated by their energy channel, then are acquired into the memory at the ad-

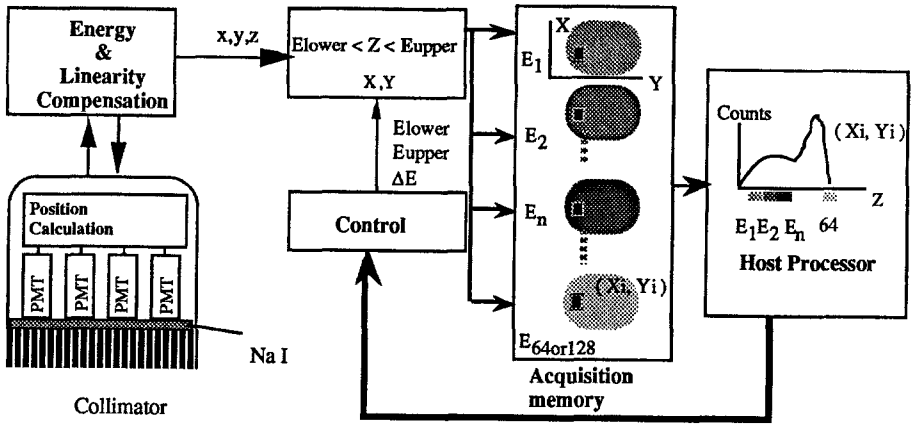

Fig. 2. Block diagram of the regional energy spectrum acquisition system

dress for (*X, Y, n*). The acquired image is split into separate images for each increment of energy width (ΔE), then transferred to the host processor. The regional energy spectrum for the position specified (*Xi, Yi*) is obtained from the pixel value of a this position (*Xi, Yi*). In each of the transferred images, the position specification and energy range setting for imaging after spectrum acquisition are performed in the host processor. The energy resolution for the regional energy spectrum at each pixel was 9.2% for ^{99m}Tc (140 keV). Photopeak channel fluctuation was found to be negligible using a ^{99m}Tc flood source. Energy spectrum acquisition conditions were as follows: energy window=10 keV (E_{lower}) to 214.8 keV (E_{upper}); number of channels=128 (1.6 keV/channel); image matrix size=128×128; one frame/channel. For both separate and simultaneous SPET/TCT scans, the regional energy spectrum for the transmission projection data at each pixel was measured to investigate the characteristics of the scattered photons.

Evaluation was performed at two positions: through the longest path of the brain phantom and through air only (shown in Fig. 2).

Simultaneous acquisition using the TEW scatter compensation method. Data acquisitions were performed in two patterns: separate or simultaneous SPET/TCT scans. ^{201}Tl and ^{99m}Tc were used for the transmission source in separate SPET/TCT scans, to evaluate the conversion method from the attenuation coefficient at 75 keV to the attenuation coefficient at 140 keV.

Radiotracers labelled with both ^{99m}Tc and iodine-123 are used in brain SPET studies. As the photopeak energy of gadolinium-153 (98 and 103 keV) is lower than that of ^{99m}Tc or ^{123}I and the half-life of ^{153}Gd is long (242 days), ^{153}Gd is the most appealing transmission source in simultaneous SPET/TCT scans. However, ^{153}Gd cannot be used at our institution. Thus, ^{201}Tl was used instead of ^{153}Gd, both of the aforementioned have photon energies lower than the emission radionuclides (e.g. ^{99m}Tc). As the 135-keV and 167-keV photopekas of ^{201}Tl overlap the ^{99m}Tc photopeak (140 keV), the contamination from ^{201}Tl to ^{99m}Tc must be compensated. The method using ^{201}Tl as the TCT source was more complicated than that using ^{153}Gd with regard to the scatter and contamination compensation. Therefore, if the method using ^{201}Tl as TCT source could be applied in the simultaneous SPET/TCT scan in this work, it would suggest that the proposed method could also be applied using ^{153}Gd as the TCT source.

The cross-talk from ^{201}Tl (135-keV photopeak) in the ^{99m}Tc window (123.2–156.8 keV) can be estimated and removed as follows:

1. The ^{201}Tl decay ratio of 75-keV Hg X-rays to the 135-keV photopeak is 96 to 3. If the difference of the attenuation coefficient of the 75-keV photons and 135-keV photons is ignored, then the count ratio of 75-keV Hg X-rays to the 135-keV photopeak is 96 to 3.
2. As the combination of the rod sources and the fan-beam collimators decreases the scatter component in transmission data (discussed below), the scatter component can be considered negligible. Therefore, the transmitted gamma rays from ^{201}Tl (135-keV photopeak and the cross-talk from 167 keV to the ^{99m}Tc window) were ignored [6].
3. Since the cross-talk from ^{201}Tl (135-keV photopeak) in the ^{99m}Tc window can be estimated at 3/96 of the measured 75-keV X-rays, this estimated cross-talk can be removed from the ^{99m}Tc projection data.

The scatter component in ^{99m}Tc SPET can be eliminated pixel by pixel using the TEW method. In addition, both scatter of ^{201}Tl and spilldown from ^{99m}Tc in TCT can be removed pixel by pixel using the TEW method.

The triple-energy windows were set over the photopeaks of ^{201}Tl and ^{99m}Tc, giving six energy windows (shown in Fig. 3). The positions of the windows for ^{201}Tl are: the scatter rejection lower window, 63–66 keV; the main window, 66–84 keV; and the scatter rejection upper window, 84–87 keV. The positions of the windows for ^{99m}Tc are: the scatter rejection lower window, 119–123.2 keV; the main window, 123.2–156.8 keV; and the scatter rejection upper window, 156.8–161 keV.

Acquisition conditions were (1) matrix size 128×128, (2) 90 projections (4°/step), (3) acquisition time 30 min. The measured attenuation coefficient for water was compared to the theoretical value. As the theoretical value for the skull part was unknown, evaluation was performed using the measured value in a separate TCT scan. The proposed SPET/TCT scanning system is evaluated by comparing the measured and true radioactivity concentration (kBq/ml).

Reconstruction of attenuation coefficients. To measure the attenuation cofficients using the rod source and fan-beam collimator, a TCT data acquisition of the brain phantom was performed. Ninety images in a 128×128 matrix were acquired over 360° at 60 s per projection using a shared scan.

A blank data acquisition was performed under the same TCT scan conditions; this was a transmission scan without the object in the field of view.

The reconstruction process in respect of the TCT image was as follows:

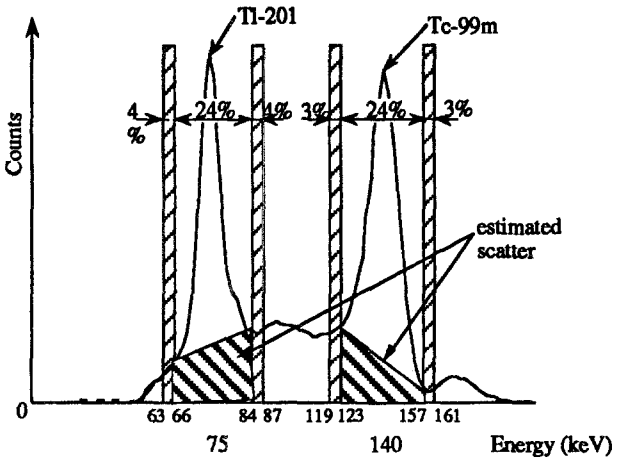

Fig. 3. Scatter and cross-contamination compensation using six energy windows and the TEW method

1. The projection data were subjected to 2D Butterworth filter processing before reconstruction (cutoff frequency 0.38 cycle/cm and order 8).
2. Attenuation coefficient projection images were formed by taking the natural logarithm of the blank-to-transmission scan ratio at each angle.
3. The TCT image was reconstructed with a fan-beam reconstruction method using filtered backprojection with a Shepp and Logan filter, and the slice thickness was 10.3 mm.
4. Since the transmission data were acquired with 75-keV photons and the emission data with 140-keV photons, the measured attenuation map was scaled by the ratio of the attenuation coefficient of water at 140 keV divided by that at 75 keV.

The TCT measured attenuation coefficients were compared with a theoretical value. The S/N properties of TCT images in water were evaluated with the normalized mean square error (NMSE) using the theoretical value as the standard value. NMSE is the root mean square error between the measured image and the standard image and is normalized with the mean square of the standard image. NMSE is expressed as the following equation:

$$\text{NMSE}\ (\%) = \sqrt{\frac{\sum (I(x,y) - S(x,y))^2}{\sum S(x,y)^2}} \times 100,$$

where $I(x,y)$ is the measured image and $S(x,y)$ is the standard image.

Reconstruction of SPET images and cross-calibration. Reconstruction of the SPET image was as follows:

1. The projection data were subjected to 2D Butterworth filter processing before reconstruction (cutoff frequency 0.38 cycle/cm and order 8).
2. The SPET image was reconstructed with a fan-beam reconstruction method using a Shepp and Logan filter, and the slice thickness was 10.3 mm.
3. Attenuation compensation was performed with a single iteration Chang algorithm that was modified to incorporate a measured non-uniform attenuation map [18].

Cross-calibration was carried out as follows:

1. SPET acquisition was performed using a fine cylinder (5 mm in diameter, 50 mm long) filled with a radioisotope of known radioactivity,
2. Scatter compensation was performed using the TEW method.
3. Attenuation compensation was performed with a single iteration Chang algorithm using the attenuation map of a 5-mm-diameter circle. The reconstruction volume included the whole range of the fine cylinder,
4. The cross-calibration factor (kBq×s/count) was calculated using the total counts of the SPET image including the whole range of the fine cylinder, the known radioactivity and the acquisition time:

   Cross-calibration factor (kBq×s/count)=radioactivity (kBq) ×acquisition time [s]/counts (count).

5. The measured specific radioactivity concentration was obtained using the cross-calibration factor, pixel length, slice thickness and acquisition time.

Evaluation of compensated SPET images. The proposed method of quantitative SPET measurement was evaluated in comparison with two other methods employing either broad-beam uniform attenuation compensation [13] or narrow-beam uniform attenuation compensation. The broad-beam uniform attenuation compensation method was applied to the SPET data without scatter compensation. The attenuation coefficient of the broad-beam method was determined empirically using a 20-cm-diameter cylinder phantom filled uniformly with ^{99m}Tc in water. The attenuation map of the broad-beam method was obtained by replacing the TCT image values of both water and skull with the empirically determined attenuation coefficient. The narrow-beam uniform attenuation compensation was applied to the scatter-compensated SPET data with the TEW method. The attenuation map of the narrow-beam method was obtained by replacing the TCT values of both water and skull with the theoretical attenuation coefficient of water.

Results

The scatter component in the separate TCT scan using regional energy spectrum acquisition

The regional energy spectra in the separate TCT scan using a fan-beam collimator and a ^{201}Tl external line source were measured using a regional energy spectrum acquisition. The measured regional energy spectra are shown in Fig. 4 at selected pixels which were through the longest path of the brain phantom and through air only. The energy spectra through the brain phantom and through air were different in magnitude due to attenuation, but were almost the same shape. This indicated that the use of a fan-beam with an uncollimated line source results in a low transmission scatter fraction. Therefore, the narrow-beam attenuation coefficient could be obtained with the proposed TCT scan system using a fan-beam collimator and a rod source without a slit collimator, and scatter compensation was not needed in the separate TCT scan.

The scatter component in the simultaneous TCT scan using regional energy spectrum acquisition

The regional energy spectra measured in the simultaneous scan for the transmission projection image at se-

lected pixels are shown in Fig. 5. This result shows much contamination from emission into transmission and the relatively weak transmission signal is almost overwhelmed by scatter from the ^{99m}Tc emission photons. The positions of the six energy windows for the TEW method are also shown in Fig. 5. As there was little overlap of the ^{99m}Tc photopeak window and the 167-keV ^{201}Tl photons, spill-down photons from 167-keV ^{201}Tl to the ^{99m}Tc photopeak window were ignored. This figure shows cross-contamination compensated emission photons and transmission photons as true emission photons and true transmission photons respectively.

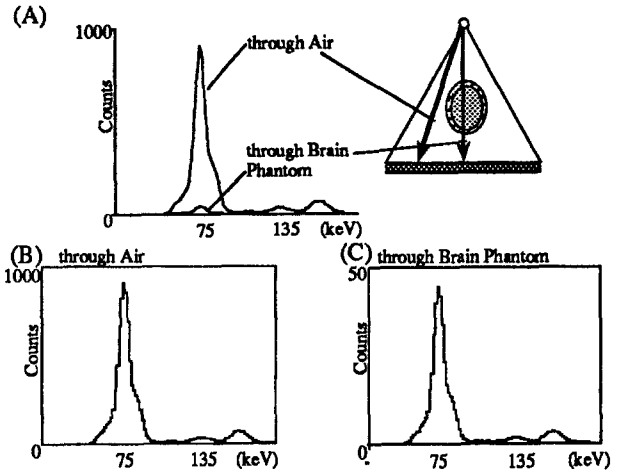

Fig. 4. Comparison of the measured regional energy spectrum from a ^{201}Tl external TCT source at the same pixel for an acquired projection image (**A**) through air/brain phantom with the same scale, (**B**) through air and (**C**) through brain phantom

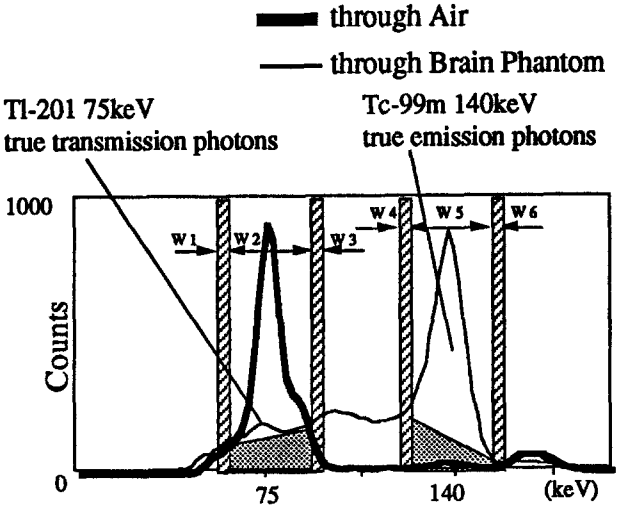

Fig. 5. Measured energy spectra in a simultaneous scan. The *bold line* is through air and the *fine line* is through a brain phantom. The positions of the windows for ^{201}Tl are: scatter rejection lower window W1, 63–66 keV; main window W2, 66–84 keV; scatter rejection upper window W3, 84–87 keV. The positions of the windows for ^{99m}Tc are: scatter rejection lower window W4, 119–123.2 keV; main window W5, 123.2–156.8 keV; scatter rejection upper window W6, 156.8–161 keV

Reconstruction of attenuation coefficients

The measured attenuation maps of separate and simultaneous scans are shown in Fig. 6. The measured attenuation coefficients are shown in Tables 1 and 2. The theoretical attenuation coefficient of ^{201}Tl (effective energy: 75 keV) for water is 0.187 cm^{-1}. Evaluation of transmission images was performed using NMSE. In a separate TCT scan, the measured attenuation coefficient for water was 0.19±0.01 cm^{-1} and the NMSE was 4%, while in a simultaneous scan the measured attenuation coefficient for water was 0.20±0.01 cm^{-1} and the NMSE was 8%. The measured attenuation coefficient for water agreed well with the narrow-beam (theoretical) value. In a separate SPET/TCT scan, the attenuation coefficient for skull was 0.34±0.02 cm^{-1} while in a simultaneous SPET/TCT scan it was 0.31×0.03 cm^{-1}.

Attenuation coefficients of standard bone are 0.37 cm^{-1} at 75 keV and 0.27 cm^{-1} at 140 keV [19]. Attenuation coefficients of water are 0.19 cm^{-1} at 75 keV and 0.15 cm^{-1} at 140 keV [20]. The attenuation coefficient ratio of standard bone at 75 keV and 140 keV is 0.27/0.37=0.73. That of water at 75 keV and 140 keV is 0.15/0.19=0.79. The measured attenuation coefficients of the skull of the brain phantom were 0.34 cm^{-1} at 75 keV and 0.27 cm^{-1} at 140 keV in this study (Tables 1, 2). The attenuation coefficient ratio of the skull at 75 keV and 140 keV was 0.27/0.34=0.79. These results indicate that the measured attenuation map acquired with 75-keV photon scan be scaled to the attenuation map for 140-keV photons by the ratio of the attenuation coefficient of water at 140 keV divided by that at 75 keV.

Simultaneous acquisition

SPET images compensated for scatter and attenuation are shown in Fig. 7. These SPET images are cross-calibrated and the radioactivity concentration (kBq/ml) im-

Table 1. Measured attenuation coefficients (TCT source ^{201}Tl)

Method	Tissue[a]	Skull[a]
Separate TCT	0.19±0.01	0.34±0.02
Simultaneous TCT	0.20±0.01	0.31±0.03
Theoretical value	0.187	–

[a] Unit: cm^{-1}

Table 2. Measured attenuation coefficients (TCT source ^{99m}Tc)

Method	Tissue[a]	Skull[a]
Separate TCT	0.15	0.27
Theoretical value	0.15	0.27

[a] Unit: cm^{-1}

ages are displayed. The measured radioactivity concentrations are shown in Table 3. The corresponding ROI positions are shown in Fig. 7. The results indicate that this work improved the contrast of grey matter to white matter and white matter to ventricle.

Compensated SPET images using an attenuation map obtained by a simultaneous TCT scan have almost the same image quality as compensated SPET images using an attenuation map obtained by a separate TCT scan. SPET values of each ROI 1–5 show almost the same radioactivity in separate and simultaneous scan images. SPET values in grey matter were lower than the true value and those in white matter were higher than the true value. However, the SPET value of the whole brain phantom agreed well with the true radioactivity.

Compensated SPET images using broad-beam attenuation compensation and cross-calibration have almost the same radioactivity over the whole brain as the compensated SPET images with the proposed method. However, the difference between the regional SPET values and the true radioactivities is greater with the broad-beam method than with the proposed method. The ratio of grey matter to white matter, of which the true value was 2.75, was 2.07 with the broad-beam method and 2.42 with the proposed method.

With the narrow-beam uniform attenuation method, the ratio of grey matter to white matter was 2.37, which was almost the same as with the proposed method. However, SPET images compensated using the narrow-beam method had lower radioactivities in all ROIs in the brain phantom than those compensated with the proposed method.

Discussion

It is highly desirable to reduce scattered photons in transmission measurements. The combination of a rod

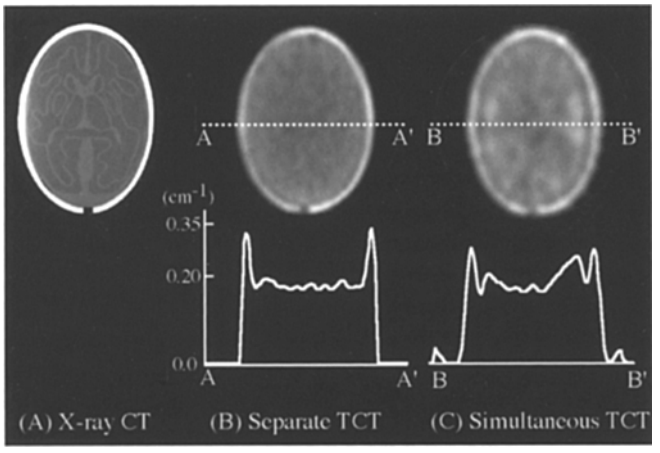

Fig. 6A–C. TCT images of brain phantom using a ^{201}Tl source. **A** Brain phantom X-ray CT image; **B** TCT image in separate scan; **C** TCT image in simultaneous scan, with scatter compensated by means of the TEW method. The profile curves of **B** and **C** are shown below

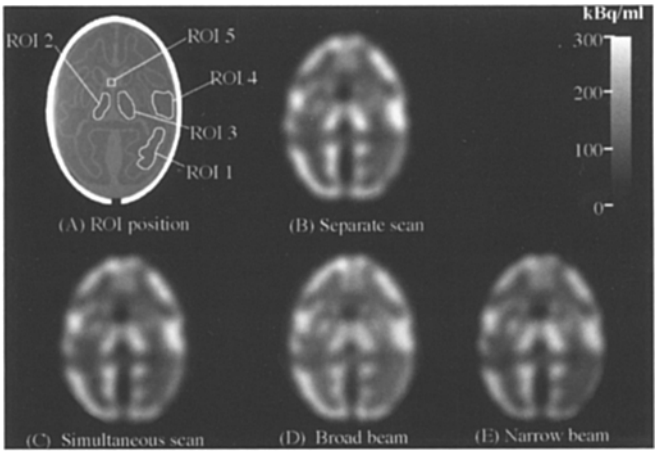

Fig. 7A–E. Cross-calibrated SPET images of brain phantom (unit: kBq/ml). **A** Brain phantom X-ray CT image and ROIs. **B** TCT and SPET measured in a separate scan. **C** TCT and SPET measured in a simultaneous scan (this work). **D** SPET using broad-beam attenuation compensation without scatter compensation. **E** SPET using narrow-beam uniform attenuation compensation with scatter compensation

Table 3. Cross-calibrated SPET value

	ROI 1	ROI 2	ROI 3	ROI 4	ROI 5	Whole activity
Separate scan	97.2 (1)	278.7 (2.87)	309.7 (3.19)	303.1 (3.12)	0.0 (0.0)	183.2 MBq
Simultaneous scan This work	95.4 (1)	271.1 (2.84)	297.4 (3.11)	315.0 (3.30)	0.0 (0.0)	177.6 MBq
Broad beam	121.5 (1)	242.9 (1.99)	268.5 (2.21)	282.3 (2.32)	34.2 (0.0)	172.7 MBq
True value	109.0 (1)	300.0 (2.75)	300.0 (2.75)	300.0 (2.75)	0.0 (0.0)	191.7 MBq

Units for ROIs are kBq/ml
The ratios to ROI 1 are shown within parentheses

(line) source and a fan-beam collimator for TCT reduces the scattered photons in transmission data. The results of regional energy spectrum acquisition indicate that fan-beam TCT using a rod source without a slit collimator reduced the detection of scattered photons. The amount of scattered photons was sufficiently low for measurements of attenuation coefficients for practical attenuation compensation. The results of regional energy spectrum acquisition showed the same shape of the energy spectrum through the brain phantom and through air. In the simultaneous method, due to the combination of emission and transmission radionuclides, cross-contamination compensation of transmission and emission data is necessary. The amount of scatter depends on the radioactivity, the kind of radionuclides and the shape of the object. The measured regional energy spectra allowed visual evaluation of the effect of cross-contamination in the simultaneous emission and transmission scan and the effectiveness at compensation using the TEW method. The regional energy spectrum acquisition mode is considered to be a good tool for the evaluation of the quantitative approach in SPET studies.

The measured ^{99m}Tc energy spectrum indicated that lead X-rays were little contaminated in the 75-keV ^{201}Hg energy window (shown in Fig. 5). As the measured attenuation coefficients (shown in Table 1) indicated good results without compensation for lead X-rays, the lead X-rays seemed not to influence the TCT image using fan-beam collimation, possibly because the fan-beam geometry might increase the self-shielding effect against lead X-rays.

As a result of this study, the following three merits of the proposed detector and fan-beam collimator geometry were demonstrated:

1. Simultaneous SPET and TCT brain study scans can be performed with a 120° shared scan using conventional fan-beam collimators. The proposed system requires less than one-third of the scanning time of the single-head system.
2. Fan-beam TCT using a rod source without a slit collimator reduces the detection of scattered photons. It provides narrow-beam attenuation measurements of the subjects.
3. The radioactivity of the external source was 85 MBq/rod (2.43 MBq/axial cm) of ^{201}Tl in this work. This is one-tenth of that in previous investigations, in which ^{99m}Tc radioactivity in a line source reported to range betwen 30 and 60 MBq/axial cm [7] or between 6.8 and 125 MBq/axial cm [12].

Since the TEW method requires only the information containd in the energy spectrum (this information was obtained using two narrow scatter rejection windows), the scatter components (cross-contamination) of emission and transmission data were easily reduced, without prediction of scatter distribution. With regard to cross-contamination in dual-isotope studies, the simultaneous SPET/TCT scans with dual isotopes are no different from dual-isotope SPET scans. The TEW method can be applied to multiple isotope studies [9]. These facts and the results of this work suggest that where the transmission radionuclides have higher photon energy than the emission radionuclides (e.g., ^{153}Gd and ^{201}Tl, respectively), cross-contamination is well compensated by the TEW method. After scatter and attenuation compensation, SPET images are displayed in kBq/ml using cross-calibration (Fig. 7).

Compensated SPET images were evaluated using five ROIs positioned at the white matter, grey matter and ventricle of the brain phantom (Fig. 7). The true values in the white matter, grey matter and ventricle were 109, 300 and 0, respectively. Compensated SPET images using an attenuation map obtained by a simultaneous TCT scan have almost the same image quality as compensated SPET images using an attenuation map obtained by a separate TCT scan. SPET values at ROIs 1–5 show almost the same radioactivity in both separate and simultaneous scan images. Results show the cross-calibrated SPET values (in kBq/ml) of the cortex, white matter and ventricle to be 110–120, 250–300 and 0, respectivly, SPET values in the grey matter were lower than the true values and those in the white matter were higher than the true values. However, the radioactivity of the whole brain phantom agreed well with the true radioactivity. Therefore, the difference between SPET values and true values and true values was thought to be due to the partial volume effect.

Compensated SPET images using broad-beam attenuation compensation and cross-calibration had almost the same radioactivity overthe whole brain as the scatter- and attenuation-compensated SPET images. However, the regional radioactivities of the grey matter, white matter and ventricle did not agree with the true radioactivities. Scatter and attenuation compensation in this work improved the contrast of grey matter to white matter. The ratio of grey matter to white matter, of which the true value was 2.75, was 2.07 with the broad-beam method and 2.42 with the proposed method. The obtained ratio indicates that the broad-beam method results in SPET images of low contrast.

As with the narrow-beam method the ratio of grey matter to white matter was 2.37, the narrow-beam method could provide the same level of contrast as the proposed method. However, SPET images compensated using the narrow-beam method had lower radioactivities in all ROIs in the brain phantom than those compensated with the proposed method. This could have resulted from underestimation of the attenuation coefficient in the skull due to the differences between the measured TCT map and the narrow-beam map. In this work, the TCT image obtained by the proposed method was used to obtain an accurate outline of the attenuation map in both the broad-beam and the narrow-beam method. It would be difficult to obtain an outline of the attenuation map using SPET data without the TCT image. As the radiotracer HMPAO is distributed in the skin of the head, accurate outline of the attenuation map could be ob-

tained by SPET data including the skull; however, the radiotracers ^{99m}Tc-ethyl cysteinate dimer and ^{123}I-iodoamphetamine are not distributed in the skin of the head, and the outline of the attenuation map would be smaller than the true outline, resulting in greater underestimation.

In conclusion, these results indicate that the proposed system improves quantitative accuracy in brain SPET. The results show the feasibility of simultaneous SPET and TCT scanning using the proposed detector and fan-beam collimator geometry to obtain quantitative brain SPET images.

References

1. Jaszczak RJ, Chang LT, Stein N, Moore FE. Whole-body single photon emission computed tomography using dual, large-field-of view scintillation cameras. *Phys Med Biol* 1979; 24: 1123–1143.
2. Morozumi T, Nakajima M, Ogawa K, Yuta S. Attenuation correction method using the information of attenuation distribution for single photon emission. CT. *Med Imag Tech* 1984; 2: 20–28.
3. Greer KL, Harris CC, Jaszczak RJ, et al. Transmission computed tomography data acquisition with a SPECT system. *J Nucl Med Tech* 1987; 15: 53–56.
4. Tung CH, Gullberg CH, Zeng GL, Christian PE, Datz FL, Morgan HT. Non uniform attenuation correction using simultaneous transmission and emission converging tomography. *IEEE Trans Nucl Sci* 1992; 39: 1134–1143.
5. Daily DL, Hutton BF, Walker PJ. Improved SPECT using simultaneous emission and transmission tomography. *J Nucl Med* 1987; 28: 844–851.
6. Fery EC, Tsui BMW, Perry R. Simultaneous acquisition of emission and transmission data for improved thallium-201 cardiac SPECT using a technetium-99m transmission source. *J Nucl Med* 1992; 33: 2238–2245.
7. Jaszczak RJ, Gilland DR, Jang S, Greer KL, Coleman RE. Fast transmission CT for determining attenuation maps using a collimated line source, rotatable air-copper lead attenuators and fan-beam collimation. *J Nucl Med* 1993; 34: 1577–1586.
8. Tan P, Bailey DL, Meikle SR, Eberl S, Fulton RR, Hutton BF. A scanning line source for simultaneous emission and transmission measurements in SPECT. *J Nucl Med* 1993; 34: 1752–1760.
9. Ichihara T, Ogawa K, Motomura N, Kubo A, Hashimoto S. Compton-scatter compensation using the triple energy window method for single and dual isotope SPECT. *J Nucl Med* 1993; 34: 2216–2221.
10. Ogawa K, Ichihara T, Kubo A. Accurate scatter correction in single photon emission CT. *Ann Nucl Med Sci* 1994; 6: 145–150.
11. Kouris K, Clarke GA, Jarrit PH, Townsend CE, Thomas SN. Physical performance evaluation of the Toshiba GCA-9300A triple-headed system. *J Nucl Med* 1993; 34: 1778–1789.
12. Kemp BJ, Prato FS, Nicholson RI, Reese L. Transmission computed tomography imaging of the head with a SPECT system and a collimated line source. *J Nucl Med* 1995; 36: 328–335.
13. Gilland DR, Jaszczak RJ, Jang S, Greer KL, Coleman RE. Quantiative SPECT reconstruction of iodine-123 data. *J Nucl Med* 1991; 32: 527–533.
14. Ogawa K, Harata Y, Ichihara T, Kubo A, Hashimoto S. A practical method for position-dependent Compton scatter correction in SPECT. *IEEE Trans Med Imaging* 1991; 10: 408–412.
15. Meikle SR, Hutton BF, Bailey DL. A transmission-dependent method for scatter correction in SPECT. *J Nucl Med* 1994; 35: 360–367.
16. Floyd CE, Jaszczak RJ, Harris CC, Coleman RE. Energy and spatial distribution of multiple order Compton scatter in SPECT: a Monte Carlo investigation. *Phys Med Biol* 1984; 29: 1217–1230.
17. Gullberg GT, Tung CH, Zeng GL, Christian PE, Datz FL, Morgan HT. Simultaneous transmission and emission computed tomography using a three-detector SPECT system. *J Nucl Med* 1992; 33: 901.
18. Ogawa K, Takagi Y, Kubo A, et al. An attenuation correction method of single photon emission computed tomography using gamma ray transmission CT. *Jpn J Nucl Med* 1985; 22: 477–490.
19. International Commission on Radiological Protection. *Report of the Task Group on Reference Man.* ICRP Publication 23. Oxford New York: Pergamon Press, 1975.
20. Hubbell JH. Photon mass attenuation and energy absorption coefficients from 1 keV to 20 MeV. *Int J Appl Radiat Isotop* 1984; 33: 1269–1290.